Journal of Earthquake Engineering
Publication details, including instructions for authors and subscription information:
http://www.tandfonline.com/loi/ueqe20

# Direct Displacement-Based Design of Glulam Timber Frame Buildings

Daniele Zonta [a], Cristiano Loss [a], Maurizio Piazza [a] & Paolo Zanon [a]
[a] Department of Mechanical and Structural Engineering, University of Trento, Trento, Italy

Version of record first published: 01 Apr 2011.

To cite this article: Daniele Zonta, Cristiano Loss, Maurizio Piazza & Paolo Zanon (2011): Direct Displacement-Based Design of Glulam Timber Frame Buildings, Journal of Earthquake Engineering, 15:3, 491-510

To link to this article: http://dx.doi.org/10.1080/13632469.2010.495184

*Journal of Earthquake Engineering*, 15:491–510, 2011

ISSN: 1363-2469 print / 1559-808X online
DOI: 10.1080/13632469.2010.495184

Taylor & Francis
Taylor & Francis Group

# Direct Displacement-Based Design of Glulam Timber Frame Buildings

DANIELE ZONTA, CRISTIANO LOSS, MAURIZIO PIAZZA, and PAOLO ZANON

Department of Mechanical and Structural Engineering, University of Trento, Trento, Italy



*We introduce a direct Displacement-Based Design methodology for glued laminated timber portal frames with moment-resisting doweled joints. We propose practical expressions to estimate ultimate target displacement and equivalent viscous damping, and we demonstrate that these expressions provide prior values that are close to those obtained a posteriori using a more refined model. Applied to case studies, the method yields base-shear forces lower than those obtained using the force-based approach of Eurocode 8. This is due to the high dissipation capacity of the specific connection technology, which apparently is conservatively accounted for in the q-factor of Eurocode 8.*

**Keywords** Displacement-Based Design; Wood Structures; Portal Frame; Moment-Resisting Joint; Target Displacement; Equivalent Viscous Damping; Dowel Connections

## 1. Introduction

Seismic codes, as applied to timber structures, sometimes appear to be excessively conservative when compared to the actual field performance during an earthquake (see, for example, Foliente, 1995). Indeed, timber structures exhibit features that allow them to resist seismic events, such as a favorable strength/density ratio and high flexibility. Their real weak point is the uncertainness associated with their ductility capacity. The timber material itself exhibits a modest ductility in compression and a typically fragile behavior in traction, in particular when load is applied perpendicular to grain. A large part of the post-elastic resources of timber buildings relies on the type of connections and on their degree of redundancy and in many cases there is an objective difficulty in predicting the actual ductile capacity. This uncertainness very often results in conservative code provisions.

It is the opinion of the authors, that the stringency of codes current in force in Europe is partially related to the approximation intrinsic to Force-Based Design methods, where all the ductile and dissipative capacity of the structure is taken into account simply by using a force reduction factor or behavior factor (the $q$-factor of Eurocode 8; CEN, 2004a). The limits of design methods based on the $q$-factor are well known and have been clearly highlighted by Priestley [1998]. These observations were accompanied by the proposal of a new seismic design methodology, referred to as Direct Displacement-Based Design (DDBD), in contraposition to the classic Force-Based Design, commonly adopted by most of the seismic design codes currently in force.

Received 18 November 2009; accepted 18 May 2010.
Address correspondence to Daniele Zonta, Department of Mechanical and Structural Engineering, University of Trento, via Mesiano, 77, 38123 Trento, Italy; E-mail: daniele.zonta@unitn.it

Since then, abundant literature on applications of this new design approach has been produced. Most of this work refers to concrete or steel structures, while relatively few texts report applications of this new philosophy to timber structures. For instance, we mention here the fundamental research carried out by Filiatrault [Filiatrault and Folz, 2002; Filiatrault *et al*., 2003] within the CUREE Woodframe Project [http://www.curee.org/projects/woodframe]. Most of this research addresses small wood-framed residential buildings where resistance to seismic action relies on nailed plywood shear-walls. More recently, Pampanin *et al*. [2006] applied DBD to a special class of multistory buildings, built with glulam or Laminated Veneer Lumber (LVL) and an innovative type of ductile connection. All these findings, however, do not extend to that broader category of structures, widespread in Europe, including warehouses and commercial buildings, based on glued laminated timber portal frames. Indeed, for these cases, type, position, performance, and redundancy of connections are the most critical features affecting the seismic behavior of the whole building.

The work presented in this article aims to define a DDBD methodology that specifically applies to this family of structures. Within this brief, we will refer to specific case studies, the three configurations of warehouse described in detail in Sec. 2, although the general concept can be easily extended to most hyperstatic portal frame buildings. We will also refer to dowel connections, as these possibly represent the type of connection most extensively used in glulam construction technology. In Sec. 3, we provide practical expressions for estimating, at design level, quantities required in order to apply the DBD procedure, namely: target displacement, ductility demand, equivalent damping to ductility relationship. In Sec. 4, we apply the DBD method to the case studies investigated, and we compare the outcomes with those obtained through the force-based approach adopted by Eurocode 8. Some concluding remarks are provided at the end of the article.

Understanding the behavior of dowel-wood connections is critical for defining a suitable seismic response model for the type of building investigated. The load-carrying capacity of a dowel connection can be easily estimated using the well established Johansen theory [Johansen, 1949], sometimes referred to as *European Yield Theory*. Because of its simplicity and accuracy, this formulation is almost universally acknowledged by design codes, including Eurocode 5 [CEN, 2004b]. However, Johansen's model provides only the strength of the connection, but no information on load-slip relation, ductile capacity, or energy dissipation of the fastener. More generally, no commonly accepted method for predicting precisely the ductile capacity of a fastened connection can be found in the scientific literature, although there are many works that deserve to be considered. The problem is closely connected to the large number of parameters necessary to characterize the general behavior of the fastening, including the angle between the load direction and the grain, the direction of the load (tension or compression), the ratio between the length and the diameter of the fasteners and obviously the number of shear planes involved. Moreover, fastener behavior is usually represented by a bi-linear law, which implies univocal definition of both yield point and ductility. However, the concepts of yield point and ductility are not well defined (see a review on this topic in appendix B of Dolan *et al*., 1994).

There has been much experimental testing of dowel connections [Dolan and Gutshall, 1997; Anderson, 2001; Heine, 2001; Smith *et al*., 1998, 2005; Daneff *et al*., 1996]. These tests underline that the variability of the connection characteristics, as to fastener diameter and to wood density, is the discriminating factor characterizing connection behavior. The tests also show that the connection performance is extremely sensitive to the load protocol, monotonic, or reversed cyclic, see for example, Dolan and Gutshall [1997] or Daneff *et al*. [1996]. Some models for describing the load-slip relationship have also been proposed. [Patton-Mallory *et al*., 1998; Heine and Dolan, 2001; Chui *et al*., 1998], most of them

based on Foschi's model [Foschi and Bonac, 1974] for reproducing the lateral penetration of the fastener.

## 2. Description of the Case Study

The structural concept selected as a case study in this article is of the type shown in Fig. 1, taken from Piazza *et al*. [2005]. This is a typical glulam warehouse built completely, as to structural members, of glulam timber of type GL24h [CEN, 2000]. Structure scheme and the main geometrical features of the portal are shown in Fig. 2. In detail, the building is a single-story structure, where all the masses are placed approximately at the same height.

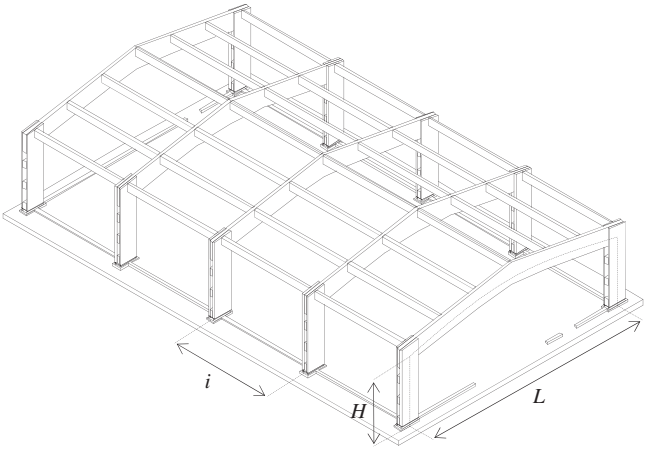


**FIGURE 1** Structure of portal timber frame building selected as case study [Piazza *et al*., 2005].

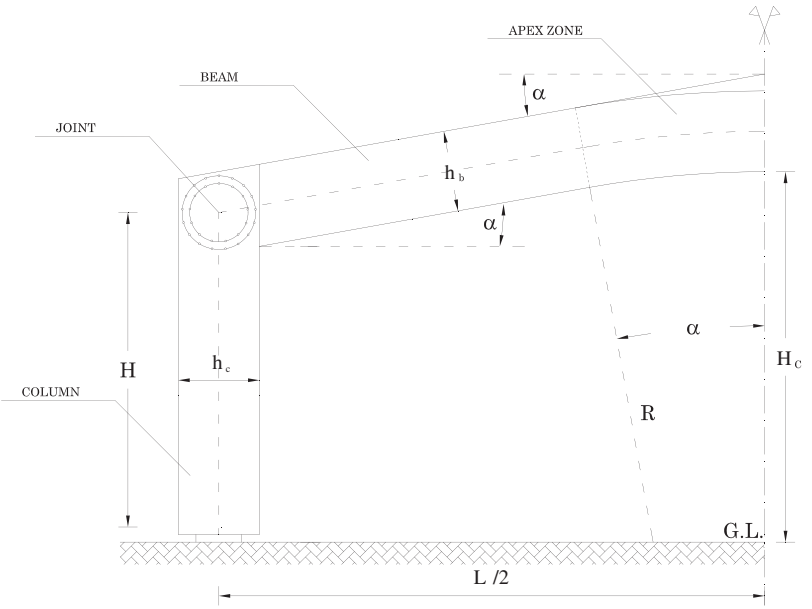


**FIGURE 2** Geometric features of the prototype portal.

The bearing structure is regular and has 5 portal frames, equally spaced at pitch 6.5 m. Each portal frame consists of a continuous curved beam with a slope $\alpha = 10.2°$ and with columns hinged at the base to the foundation. The columns have spaced elements connected with packs. The beam has a non structural part at the top of the apex zone, in order to reduce the values of stress orthogonal to grain. The secondary structure of the roof consists of six beams and a ridge beam of identical cross section, all manufactured with glued laminated timber. Plywood panels are infilled between the columns serving as shear walls, while the roof in-plane bracing is provided by the timber boarding.

In order to cover the variability of the geometrical dimensions of the portal, in this article we will investigate three different configurations, labeled A, B, and C. The geometrical dimensions of these buildings are shown in Fig. 3 and reported in detail in Table 1. Case B is a warehouse of average size (5.22 m high and 14.4 m wide), typically used for commercial purposes. Cases A and C represent the lower and upper limits of geometrical dimensions of the portal, suitable for this construction technology.

These buildings are all dimensioned according to Eurocodes: in detail, we assumed a service class 1, according to Eurocode 5, and seismic zone with a ground type C and a design ground acceleration $a_g = 0.35$ g, according to Eurocode 8. For seismic design, the total mass of a portal is considered as concentrated at the roof level. In this article, the analysis addresses only the in-frame direction, assuming that, as in real-life building, the seismic load in the other direction is born by classic sway brace systems [Piazza *et al*., 2005].

In all cases, the beam to column connection is a moment resisting joint fastened with dowels located on two concentric circles (see Fig. 4). The dowels work as double shear plane, timber to timber connections. The joint also includes other types of steel fasteners which have only a tightening function, and for this reason are not considered in the following discussion. Assuming the members to be rigid, the elastic rotational stiffness of the

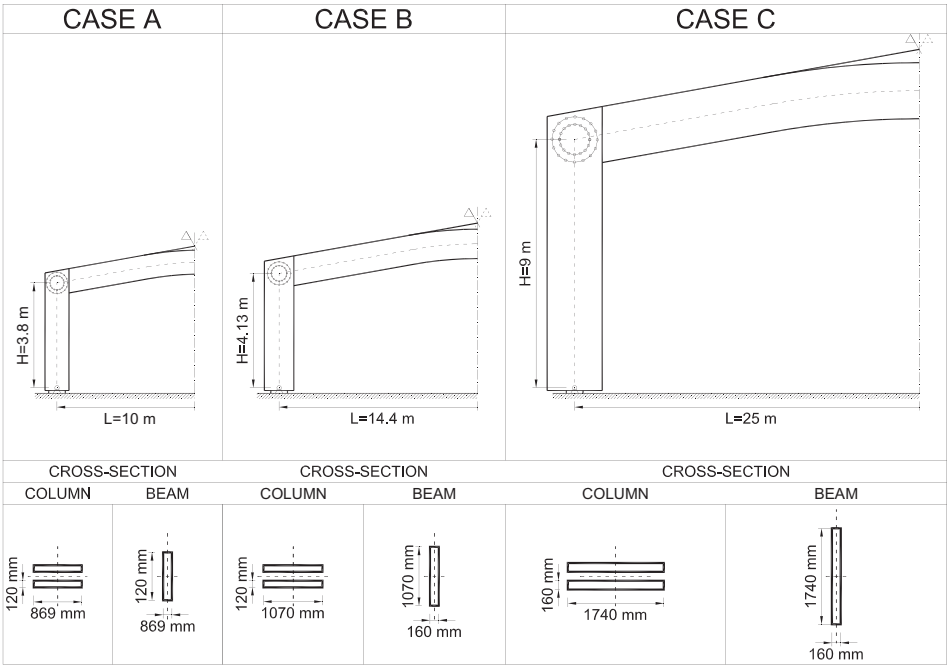


**FIGURE 3** Geometrical dimensions of the three case studies investigated.

**TABLE 1** Geometrical and mechanical parameters of the three cases investigated

| | CASE A | | CASE B | | CASE C | |
|---|---|---|---|---|---|---|
| | *Design I* | *Design II* | *Design I* | *Design II* | *Design I* | *Design II* |
| *Geometrical dimensions of the portal* | | | | | | |
| Nominal height of the portal – $H$ [m] | 3.8 | 3.8 | 4.1 | 4.1 | 9 | 9 |
| Maximum clearance of the portal – $H_C$ [m] | 4.53 | 4.53 | 5.22 | 5.22 | 10.75 | 10.75 |
| Nominal width of the portal – $L$ [m] | 10 | 10 | 14.4 | 14.4 | 25 | 25 |
| Slope of the roof beam – $\alpha$ [°] | 10.2 | 10.2 | 10.2 | 10.2 | 10.2 | 10.2 |
| Radius of the roof beam – $R$ [m] | 11 | 11 | 13 | 13 | 30 | 30 |
| Thickness of the beam – $b_b$ [mm] | 160 | 160 | 160 | 160 | 160 | 160 |
| Thickness of the column – $b_c$ [mm] | 2 ×120 | 2 × 120 | 2 × 120 | 2 × 120 | 2 × 120 | 2 × 120 |
| Height of the beam cross-section – $h_b$ [mm] | 869 | 869 | 1070 | 1070 | 1740 | 1740 |
| Height of the column cross-section – $h_c$ [mm] | 869 | 869 | 1070 | 1070 | 1740 | 1740 |
| *Geometrical dimensions and mechanical properties of the joint* | | | | | | |
| Dowels diameter – $d$ [mm] | 12 | 16 | 12 | 16 | 12 | 16 |
| Radius of the internal dowel crown – $r_{int}$ [mm] | 325 | 290 | 425 | 385 | 760 | 725 |
| Radius of the external dowel crown – $r_{ext}$ [mm] | 385 | 370 | 485 | 465 | 820 | 805 |
| Number of internal dowels – $n_{int}$ | 34 | 22 | 44 | 30 | 79 | 56 |
| Number of external dowels – $n_{ext}$ | 40 | 29 | 50 | 36 | 85 | 63 |
| Elastic rotational stiffness – $K_{\varphi es}$ [kNm rd$^{-1}$] | 84600 | 69000 | 175200 | 148300 | 913700 | 832700 |
| Ultimate rotational stiffness – $K_{\varphi u}$ [kNm rd$^{-1}$] | 56400 | 46000 | 116800 | 98900 | 609100 | 555200 |

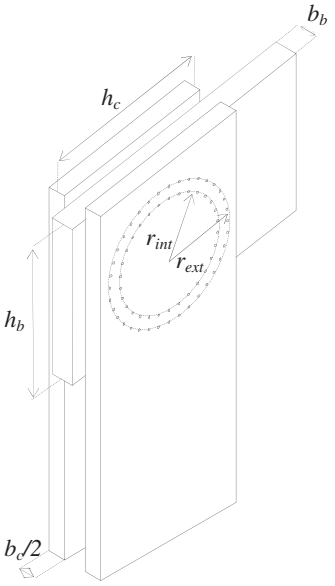


**FIGURE 4** Moment resisting joint.



joint $K_\varphi$, i.e., the constant that relates moment $M$ to rotation $\Delta_\varphi$, can be easily calculated with the classic expression:

$$K_\varphi = \sum_i^n K_i r_i^2 \,, \tag{1}$$

where $K_i$ is the elastic slip modulus of the $i$-th single dowel and $r_i$ is its distance from the geometrical center of the fasteners. Within the scope of this work, the slip modulus of the single fastener can be conventionally assumed equal to that given by Eurocode 5. Table 1 illustrates how we can obtain almost identical static performance of the connection by arranging in similar configuration either dowels with diameter $d = 12$ mm (*Design I*) or of diameter $d = 16$ mm (*Design II*). Indeed, for each case, both the designs are equally well assessed with respect to the maximum shear action at the most critical dowel, under static loads. However, the base shear calculated according to Eurocode 8 is very sensitive to dowel diameter. Eurocode 8 states specifications for defining the most appropriate ductility design class, L, M, or H, based on the joint detailing. Design in ductility class H is allowed when the fastener diameter $d$ does not exceed 12 mm and the thickness $t$ of the connected members is not less than 10 times $d$: in this case, a value of $q = 4$ can be assumed. By contrast, when $d$ is greater than 12 mm and $t$ is less than 8 times $d$, the structure should be classified in ductility class L, and a value as low as $q = 1.5$ must be taken. It is immediately verified that in our case, being $t = 120$ mm, the first condition is fulfilled using dowels with diameter $d = 12$ mm as in *Design I*; the latter when $d = 16$ mm as in *Design II*. This results in a completely different base shear force calculated in the two scenarios, *Design I* and *Design II*, respectively, as will be illustrated later on in Table 3.

## 3. Formulation of a DBD Method for Timber Portal Structures

This sharp difference in the seismic performance of the two designs is obviously due to the rough ductile classification of Eurocode 8, typically resulting in conservative provisions. However, this is also in part the consequence of the roughness of the $q$-factor method itself. In this section, we introduce a DDBD formulation that specifically applies to timber portal-frame structures; in essence, this is an extension to glulam frames of the general methodology developed by Priestley [2003] for concrete and steel structures. Application of this method requires estimation of (i) the target displacement $\Delta_d$ of the portal and (ii) the equivalent damping ratio $\xi_d$ of the structure at the ultimate capacity. Practical expressions for these parameters are provided in Secs. 3.1 and 3.2, respectively.



### *3.1. Target Displacement*

A necessary condition for applying the DBD method is that it be somehow possible to estimate *a priori* the target displacement $\Delta_d$ of the portal, regardless of the geometrical dimensions of members and connections. In the case of serviceability limit states, this condition normally applies, as the limit value of displacement is typically expressed in terms of maximum acceptable drift of the building (see, for example, Eurocode 8 provisions).

For an ultimate limit state, this estimate might not be so obvious, because the ultimate capacity generally depends on member and joint characteristics, which are unknown at the design phase. Nevertheless, below we will show that, in the case of a two-hinged timber portal building, it is possible to obtain a priori a sufficiently accurate estimate of $\Delta_d$ using a fairly simple formulation. First of all, we can assume that, if the members are appropriately dimensioned, at ultimate limit state all of the inelastic displacement is due to rotation of the joints, while the timber member behavior is considered elastic. Hence, we can estimate the total target capacity $\Delta_d$ as the sum of the displacement $\Delta_j$ due to rigid rotation of columns, as a consequence of joint yield, and the elastic deformation $\Delta_s$ of the portal, calculated assuming the joints to be rigid (Fig. 5):

$$\Delta_d = \Delta_j + \Delta_s \tag{2}$$

Evidently, we have $\Delta_j = \varphi_u H$, where $\varphi_u$ is the ultimate rotation of a joint and $H$ the column height.

The assumption of rigid members basically means that the rotation $\varphi$ will produce, in each fastener, slips $\delta_i$ proportional to their distance from the joint centre of rotation $C$. Therefore, the ultimate limit state equation reads:

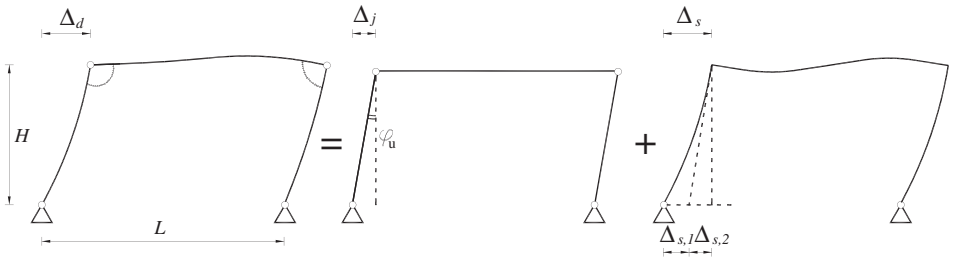


**FIGURE 5** Conceptual model for estimating the target displacement.

$$\delta_u = r_{\max}\varphi_u, \tag{3}$$

where $r_{max}$ is the maximum distance between the rotation center $C$ and the most critical dowel. For simplicity, we will assume here that all the fasteners are located in a singular circular pattern, of radius $r$. As the connection is subject to both shear $V$ and moment $M$, the rotation center $C$ does not coincide with the geometrical center $O$ of this circle. In general, the direction of shear stress depends on the ratio between seismic loads and gravitational loads: if we further assume that the gravitational loads can be neglected in this calculation, then the relation $M = VH$ must hold. With some approximation we can further assume the ultimate distribution of forces on dowels to be proportional to that in the elastic state. Hence, moment and shear components of dowel reaction can be calculated using:

$$F_M = \frac{M}{nr}; \quad F_V = \frac{V}{n}, \tag{4}$$

where $n$ is the total number of dowels in the connection.
Using simple geometrical relations, with reference to Fig. 6, and keeping in mind that $M = VH$, we obtain the following estimate of $r_{max}$:

$$\Delta r = r\frac{F_V}{F_M} = r^2\frac{V}{M} = \frac{r^2}{H} \qquad r_{\max} = r + \Delta r = r\left(1 + \frac{r}{H}\right) \tag{5 a, b}$$

Hence, the following expression for the ultimate rotation is found:

$$\varphi_u = \frac{\delta_u}{r\left(1 + \frac{r}{H}\right)} \tag{6}$$

The displacement $\Delta_j$ can be written as:

$$\Delta_j = \phi_u H = \frac{\delta_u}{r\left(1 + \frac{r}{H}\right)}H = \frac{\delta_u}{1 + \frac{L}{H}\frac{h}{L}\frac{r}{h}}\frac{H}{L}\frac{L}{h}\frac{h}{r} = \delta_u\frac{\theta\gamma\beta}{1 + 1/\theta\gamma\beta}, \tag{7}$$

where $h$ is the minimum section height of a member, beam, or column; $\theta = H/L$ is the aspect ratio of the building; $\gamma = L/h$ and $\beta = h/r$.

Displacement $\Delta_s$, is simply given by the elastic relation:

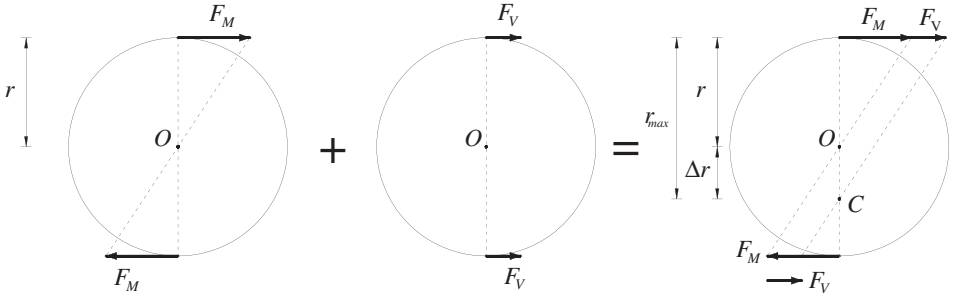


**FIGURE 6** Moment and shear stress components on dowels.

$$\Delta_s = \Delta_{s,1} + \Delta_{s,2} = \frac{MH^2}{3EJ_c} + \frac{M}{6EJ_b}LH, \tag{8}$$

where $E$ is the timber elastic modulus, and $J_b$ and $J_c$ are the moments of inertia of the beam and the column, respectively. Equation (8) depends on the member characteristics, but can be rearranged assuming some simplifications. If the portal is appropriately designed, the beam yield moment $M_{R,b}$ should be greater than the joint ultimate resisting moment $M_u$. In other words, it should be $M_u = \alpha M_{R,b}$, where $\alpha$ is an over-strength factor. Thus, Eq. (8) at the ultimate state can be rewritten as:

$$\begin{aligned}\Delta_s &= \frac{M_u}{3EJ_b}\left(\frac{J_b}{J_c}H^2 + \frac{HL}{2}\right) = \frac{HL}{3\alpha}\frac{M_{R,b}}{EJ_b}\left(\frac{H}{L}\frac{J_b}{J_c} + \frac{1}{2}\right) \\ &= \frac{HL}{3\alpha}\frac{2\varepsilon_y}{h}\left(\theta\frac{J_b}{J_c} + \frac{1}{2}\right) = \frac{2}{3\alpha}\left(\theta\frac{J_b}{J_c} + \frac{1}{2}\right)H\gamma\varepsilon_y\end{aligned} \tag{9}$$

where $\varepsilon_y$ is a conventional yield strain of timber (calculated as the ratio of nominal strength $f_m$ to Young's modulus $E$) and $\theta = H/L$ is the aspect ratio of the portal. Reasonable values for conventional yield strain and over-strength factor are $\varepsilon_y = 0.002$ and $\alpha = 1.2\text{-}1.3$, respectively. Also, for a typical warehouse building we might expect that $J_b/J_c \cong b_b/b_c = 1.0 - 0.5$. Using the conservative value of $J_b/J_c = 0.5$, the expression of $\Delta_s$ reduces to just:

$$\Delta_s \cong \frac{H}{2000}\gamma\,(\theta + 1) \tag{10}$$

In summary, by combining Eqs. (7) and (10), the ultimate target displacement can be estimated using the following simple equation:

$$\Delta_d = \delta_u\frac{\theta\gamma\beta}{1 + 1/\theta\gamma\beta} + \frac{H}{2000}\,(\theta + 1)\,\gamma \tag{11}$$

From this simple formula we can note that the parameters that control the displacement capacity of the portal are basically the ultimate slip of the dowel $\delta_u$, the height of the building $H$, the portal aspect ratio $\theta = H/L$, and the ratio $\gamma = L/h$. Also, the ratio $\beta = h/r$ influences the displacement capacity, but only to a minor extent. It is important to observe that even if Eq. (11) depends on some geometrical quantities, all these quantities are known or can be established before beginning the structural design process. $H$ and $\theta$ are obviously known at the design stage, while reasonable assumptions can be made for prior estimation of the other geometrical parameters. In fact, $\beta = h/r$ is necessarily greater than 2 and most typically somewhere between 2.5 and 3; also, under normal design assumptions, $\gamma = L/h$ is expected to be between 10 and 15. Indeed, deeper investigation and experiments are needed in order to gain more reliable knowledge of the ultimate slip of a dowel connection $\delta_u$.

### *3.2. Ductility Capacity*

Similarly to Eq. (11), we can estimate a conventional value of yield displacement using

$$\Delta_y = \delta_y\frac{\theta\gamma\beta}{1 + 1/\theta\gamma\beta} + \frac{H}{2000}\,(\theta + 1)\,\gamma\ , \tag{12}$$

where now $\delta_y$ is the dowel slip at the conventional yield point. As usual, the ductility capacity of the structure $\mu_s$ can be calculated as the ratio of $\Delta_d$ to $\Delta_y$. As mentioned in Sec. 1, there is no agreement on the definition of yield point as applied to a dowel connection, and the same uncertainty reflects in the definition of structural ductility. In this work, we conventionally define the yield slip $\delta_y$ as the ratio of the load-carrying capacity of the dowel to the modulus of slip, both of them calculated according to Eurocode 5. Therefore, the ductility values calculated later on also depend on the conventional nature of this definition. We must keep in mind this point when we apply relationships based on ductility, such as Eq. (13), to other types of timber structures.

### *3.3. Equivalent Damping Ratio*

The next step in the application the DDBD method is to define the design damping $\xi_d$, i.e., the equivalent viscous damping of the structure at the design displacement. An examination of the literature published to date shows very few works dealing specifically with damping in wood structures and, among these, Foliente [1995] and Blandon and Priestley [2005] are possibly the only sources suggesting general procedures to estimate an equivalent viscous damping. Apart from these, a number of experimental works tackle the problem of damping in certain cases and under specific conditions. Comparison of these works highlights how difficult is to define general rules that apply equally well to any type of timber structure.

For instance, Chui and Smith [1989], based on previous work, reported a range of values valid for two specific structural typologies, namely timber floors and structures assembled using nailed joints. The same authors also recognize that the dissipation capacity of a wood structure depends strongly on the type of connection and on the boundary conditions. Although not really focusing on earthquake response, an old work by Yeh *et al*. [1971] likewise deserves much attention, as it concentrates on the physical origin of damping in wooden structures. The authors identified three main sources: internal damping of material, adhesive damping at glued surfaces, and friction damping at nailed surfaces; and suggested that the three damping sources stand in the order of 1:2:6 for conventional structures. Based on experimental results on nailed wood-to-sheathing joints, Polensek and Bastendorff [1987] proposed, for this type of connection, values from 10–30%, depending on the degree of connection and the angle between load and grain. More recently, Yasamura [1996] reported values of damping of 10–20% for nailed joints under cyclic loads.

The apparent disagreement between the values proposed by different authors reflects the large variability of energy dissipation in timber structures, which is strictly dependent on the specific construction technology, as well as on the operational conditions. In general, it is commonly acceptable to see the equivalent damping rate $\xi_d$ as the sum of a constant viscous component $\xi_0$ and a hysteretic component $\xi_{hyst}$, which increases with displacement capacity $\Delta_d$. It is also customary to express the hysteretic component of damping as a function of structural ductility $\mu$. An often used general formulation of this kind is that suggested by Priestley [2003]:

$$\xi_d = \xi_0 + \xi_{hyst} = \xi_0 + \frac{a}{\pi}\left(1 - \frac{1}{\mu^{0.5}}\right), \tag{13}$$

where $a$ and $\xi_0$ are constants that depend on the structural material and technology. This expression generalizes the formulation originally proposed by Gulkan and Sozen [1974] for concrete structures. It is commonly used for steel and concrete, while almost no application is found in the technical literature in the case of timber. After all, we must remark how for wooden structures the phenomenon of stiffness degradation in cyclic loads makes the

application of this equation unavoidably approximate. Sartori [2008] proposed values for parameter $a$ and $\xi_0$ calibrated on the experimental outcomes of tests on full-scale fastened glulam joints designed for ductile failure mode (failure mode 3 according to Johansen's theory [1949]). Details of this experimental work are in turn reported in Polastri *et al*. [2008]. More specifically, the tests were carried out according to standard EN 12512 [CEN, 2001]: the load protocol specified includes a sequence of reversed cycles of increasing amplitude and is the standard used in Europe to characterize the response of fastened joints. Sartori's general assumption is that the energy dissipation of a glulam frame is mostly due to plastic deformation of its connections. We must remember at this point that, for fastened connections, the hysteretic dissipation is partially due to the steel dowels that embed in the wood during the load action. Because this mechanism implies reduction of energy dissipation after each cycle, the total amount of energy dissipated depends largely on the load protocol: and therefore, we do not expect the relationship between equivalent damping and ductility to be unique. This concept is clearly illustrated in the graph of Fig. 7, based on the experiment reported in Polastri *et al*. [2008], representing the moment-rotation relationship experimentally observed for a fastened joint under the first load cycle and under subsequent cycles.

Taking account of this issue, Sartori calculated the three different types of damping-to-ductility curves of the type shown in Fig. 8, here labeled Protocol 1, Protocol 2, and Protocol 3.

The first curve (Protocol 1) is that obtained under the same load protocol used in the experimental tests. The other two represent the upper- and lower-bound curves (Protocols 2 and 3), theoretically expected in the case of monotonically increasing cyclic load and constant amplitude cyclic load, respectively.

For the purpose of this work, the use of the first type of curve seems the most appropriate to reproduce the effect of a real earthquake, and the validity of this assumption will be verified in Sec. 4 with nonlinear time history analysis. In this case, the numerical values of the dissipation parameters are: $a = 60$ and $\xi_0 = 10\%$ for *Design I* (dissipative behavior); $a = 54$ and $\xi_0 = 8\%$ for *Design II* (low dissipative behavior). The corresponding damping-ductility curves are those reported in Fig. 9a, and will be adopted in the calculation reported in rest of this work.

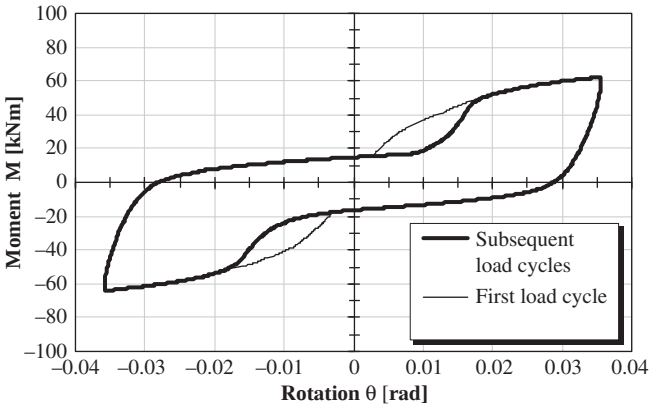


**FIGURE 7** Typical moment-rotation relationship for a doweled joint at first and subsequent load cycles, based on Polastri *et al*. [2008].

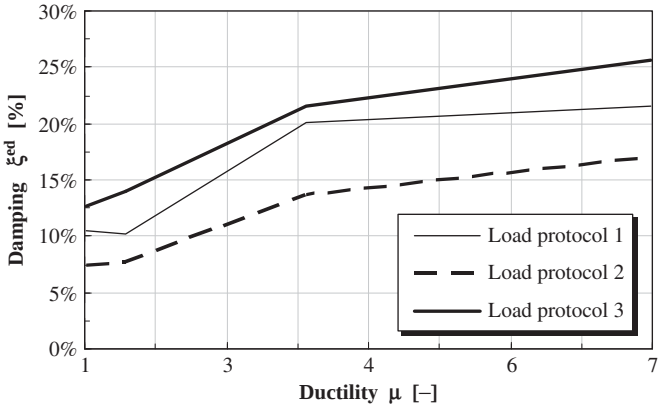


**FIGURE 8** Experimental equivalent damping vs. ductility relationships for ductile joints with 12 mm diameter dowels, based on Sartori [2008].

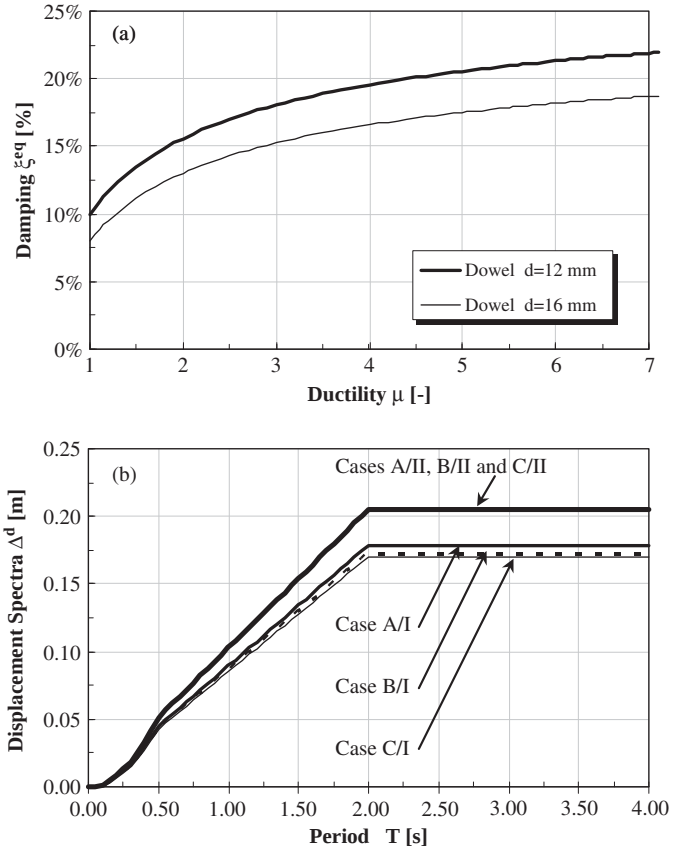


**FIGURE 9** Equivalent damping vs. ductility relationship (a) – Design displacement spectra (b).

### 3.4. Design Base Shear Force

Once defined the target displacement $\Delta_d$ and the corresponding equivalent damping $\xi_d$, the equivalent period of the structure $T_{eq}$ at the ultimate displacement is obtained solving the following limit state equation:

$$\Delta_d = S_d\left(T_{eq}, \xi_d\right), \tag{14}$$

where $S_d$ represents the expression of the elastic displacement spectra as a function of period and damping rate. Equation (14) can be solved either numerically or graphically, based on the representation of the response spectra provided, for example, by Eurocode 8. The equivalent stiffness $k_{eq}$ and the design base shear force of the structure $F_b$ can be obtained by the following expressions:

$$k_{eq} = \frac{4\pi^2 m_{eff}}{T_{eq}^2};\ F_b = k_{eq}\Delta_d, \tag{15a,b}$$

where $m_{eff}$ is the effective mass associated with the first mode shape.

## 4. Application to the Case Study

In this section, we apply the DDBD methodology described before to the three case studies, in order to compare the results with those obtained using Eurocode 8. The scope of this comparison is to highlight how the design method, force-, or displacement-based, may influence the evaluation of the base shear. To do so, we must verify that the parameters chosen in the DBD approach are consistent with the implicit assumptions of Eurocode 8.

As seen before, Eurocode 8 assigns ductility class H and a behavior factor $q = 4$ to the frame structure when the connections are fastened with $d = 12$ mm dowels, as in *Design I*. The same code assumes that in this case the dissipative zones shall be capable of plastic deformation for at least three fully reversed cycles, at a static ductility ratio of 6, with no more than 20% loss of strength. Therefore we may conservatively assume that the ultimate slip of the dowel $\delta_u$ is at least 6 times the conventional yield slip $\delta_y$. In turn, $\delta_y$ is calculated as the ratio between the yield strength $F_y$ and the slip modulus $K_\phi$, both of these given by Eurocode 5.

As for *Design II*, Eurocode 8 does not specify any information on the ductile capacity of the connections: it assumes that whenever the fastener diameter is greater than 12 mm the structure *might* undergo non ductile failure mechanisms, and conservatively imposes on the designer a behavior factor of 1.5. We cannot avoid noting here that this approach is somehow inconsistent with Johansen's theory, acknowledged by Eurocode 5, whereby in principle a joint can be designed for ductile failure regardless the diameter of the dowels. More specifically, the failure is ductile when the minimum resistance coincides with that provided by Eq. 8.8(k) of Eurocode 5. For instance, all the joints in the three configurations, A, B, and C, considered in this article are designed for ductile failure according Eurocode 5. On the other hand, we must recognize that failure mode is much more critical in seismic design than in static, and this justifies to a certain extent, the conservative provision suggested in Eurocode 8.

Nevertheless, here our objective is not to discuss the validity of the assumptions of Eurocode 8, rather to apply the DBD consistently with these assumptions. To do so, we can observe that in general the ductility capacity of the structure $\mu$ must be greater than or equal to the force reduction factor $q$: therefore, to warrant a $q$ not greater than 1.5, a value

of $\mu = 1.5$ must be conservatively assumed. Hence, in this case we can only assume the target displacement $\Delta_d$ to be 1.5 times the yield displacement of the structure $\Delta_y$, estimated using Eq. (12). Equation (11) is used in this case to calculate backwards the inherent dowel ultimate slip and eventually its ductility, obtaining values varying from 1.93–2.79, as shown in Table 2.

The ability of Eq. (11) to predict the ultimate response, based on the dowel slip capacity, has been verified case by case through a pushover analysis on non-linear finite element models of the portal, of the type shown in Fig. 10a. Each model takes account of the exact geometry of members and connections. Members are modeled as linear elements, 26–42

**TABLE 2** Base-shear forces calculated using the direct displacement-based design procedure

| | CASE A | | CASE B | | CASE C | |
|---|---|---|---|---|---|---|
| | *Design I* | *Design II* | *Design I* | *Design II* | *Design I* | *Design II* |
| Dowel yielding slip – $\delta_y$ [mm] | 2.9 | 3.7 | 2.9 | 3.7 | 2.9 | 3.7 |
| Dowel ultimate slip – $\delta_u$ [mm] | 17.1 | 7.1 | 17.1 | 7.8 | 17.1 | 9.8 |
| Dowel ductility – $\mu_\delta$ | 6 | 1.9 | 6 | 2.1 | 6 | 2.8 |
| Yielding displacement (Eq. 12) – $\Delta_y$ | 56 | 65 | 58 | 65 | 117 | 126 |
| **Target displacement (Eq. 11) – $\Delta_d$ [mm]** | **183** | **96** | **166** | **97** | **260** | **188** |
| Structural ductility capacity – $\mu$ | 3.3 | 1.5 | 2.9 | 1.5 | 2.2 | 1.5 |
| **Ultimate displacement (via pushover analysis) [mm]** | **180** | **103** | **153** | **104** | **237** | **232** |
| Equivalent viscous damping (Eq. 13) – $\xi_{eq}$ [%] | 18.5 | 11.2 | 17.8 | 11.2 | 16.3 | 11.2 |
| Equivalent viscous damping (via non linear time history analysis) – $\xi_{eq}$ [%] | 20.4 | 11.0 | 20 | 9.2 | 15.1 | 9.2 |
| Seismic mass – $W$ [Kg] | 13600 | 13600 | 19800 | 19800 | 35500 | 35500 |
| Equivalent period – $T_e$ [s] | 2.00* | 0.95 | 1.93 | 0.96 | 2.00* | 1.84 |
| Secant stiffness – $K_e$ [KN m$^{-1}$] | 114.5 | 595.2 | 210.10 | 854.3 | 165.2 | 415.7 |
| **Design base shear – $F_b$ [KN]** | **21.1** | **57.6** | **35.0** | **83.0** | **43** | **78.3** |

*Taken equal to the limit of the constant displacement field in the response spectrum $T_D = 2$s

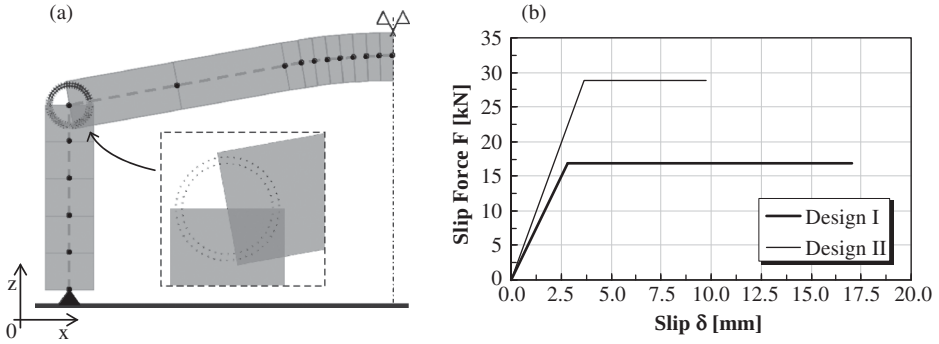


**FIGURE 10** Finite element model for nonlinear time pushover analisys (a) and load –slip model for $d = 12$ mm (*Design I*) and $d = 16$ mm (*Design II*) dowels (b).



depending on the size of the portal, while the behavior of the connection is reproduced with a set of nonlinear link elements, one per dowel, distributed in double-crown configuration as per design. Consistently with the previous discussion, the load-slip relationships for the two types of dowel are those shown in Fig. 10b. The results of the pushover analysis are reported in Fig. 11.

As far as *Design I* is concerned, the comparison demonstrates how Eq. (11), even if somewhat approximate, provides conservative prior values of target displacement that in fact are quite close to those obtained *a posteriori* using a much more refined model: the estimation error is normally lower than 10% except for case C/II where the scatter is 19%. More specifically, Eq. (11) slightly overestimates the actual displacement capacity for *Design I*, and underestimates it for *Design II*. To understand the reason for this, we must go back to Sec. 3 and remember that the target displacement formulation includes a plastic and an elastic term. While the first depends on the ultimate dowel slip only through a geometrical relationship, the latter is estimated conservatively to account for a number of quantities unknown at the design stage. Consequently, we expect the estimate of the ultimate displacement to be more conservative when, as for *Design II*, the elastic deformation is dominant. In the case of *Design I*, the slight overestimate is essentially due to the fact that Eq. (11) does not account for the gravity load, and the small errors observed confirm that this approximation is perfectly acceptable at the design phase.

The equivalent damping ratio is estimated by Eq. (13) based on the ductile capacity $\mu$ of the structure. In addition, we used a nonlinear time-history analysis to verify the ability of Eq. (13) to predict the energy dissipated by the system at the most severe displacement amplitude. The finite element model employed for the analysis is that shown in Fig. 12a. Contrary to the model used for the pushover analysis, here the behavior of the connection is reproduced by a single hysteretic rotational element, consistently with the experimental dataset which generated the coefficients of Eq. (13).

The hysteretic moment-rotation relationship selected for this application is the so-called pivot model introduced by Dowell *et al*. [1998], to which the reader is referred for more details. The input parameters of the pivot model are the first yield and the ultimate moment of the doweled connection, and the non dimensional parameters $\alpha$ and $\beta$, which set the pivot and pinching points of the system [Dowell *et al*., 1998]. While the two resisting moments are obviously determinate for each case study, the non dimensional coefficients were calibrated on the experimental moment-rotation relationship presented in Polastri *et al*. [2008], obtaining values of $\alpha = 10$ and $\beta = 0.3$. Figure 12b shows how the hysteretic model fits the experimental moment-rotation relationship.

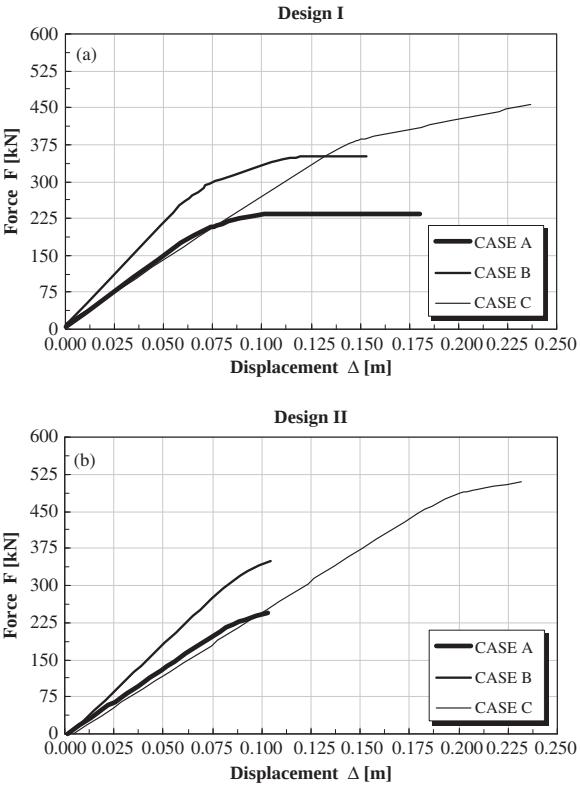


**FIGURE 11** Pushover analysis of the portal under *Design I* (a) and *Design II* (b) assumptions.

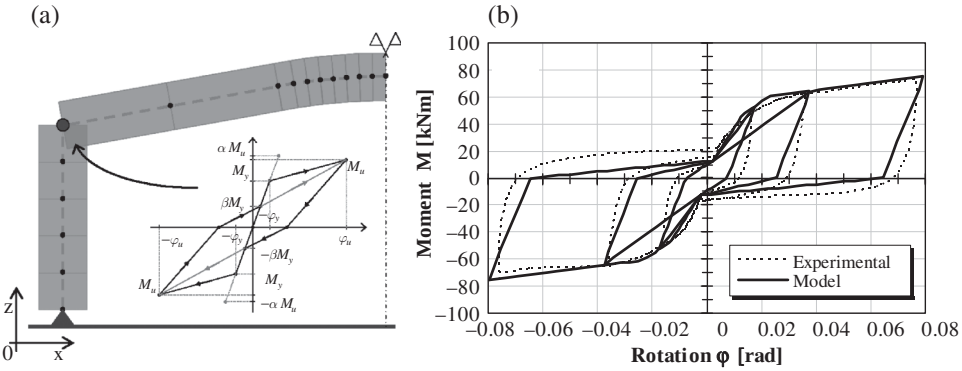


**FIGURE 12** Finite element model for nonlinear time-history analysis (a) and moment-rotation relationship for the nonlinear rotational spring (b) compared with the experimental dataset from Polastri *et al*. [2008].

The seismic input consists of a set of five artificial ground motions compatible with the same Eurocode 8 spectrum used in the design. The spectrum-compatible accelerograms are generated using SIMQKE-II [Vanmarcke *et al*., 1997] and then scaled, case by case, to produce a maximum displacement response equal to the target displacement estimated by Eq. (11). For each case study, the resulting mean value of equivalent viscous damping is reported in Table 2 along with the equivalent damping calculated by Eq. (13). By comparing of these values we can see how Eq. (13), although very simple, yields estimates of equivalent damping that are accurate enough for the purpose of the DBD.

Based on the resulting values of equivalent damping, Eurocode 8 provides displacement response spectra of the type shown in Fig. 9b, and the equivalent elastic period of the structure $T_{eq}$, based on the target displacement considered, can be read directly from this set of design displacement spectra. The design base shear forces $F_b$ are then obtained using Eq. (15b). The resulting values are all reported in Table 2.

It is worth noting that for cases A/I and C/I the ultimate displacement capacity estimated with Eq. (11) is greater than the maximum spectral displacement demand. In practical terms, this means that the portal is virtually verified whatever value of shear force is assumed in design. We considered this issue, adopting for these cases period $T_D = 2$ sec as equivalent period, being $T_D$ the limit of the constant displacement field in the response spectrum; this design choice corresponding to the maximum values of stiffness and base shear.

In a similar manner, we summarize in Table 3 the results of the seismic design carried out on the same case studies using the force-based procedure of Eurocode 8.

At this point, it is interesting to compare the values of base shear obtained using the two methodologies, force-based and displacement-based, bearing in mind that the baseline assumptions are the same in both cases. The first general observation is that the DBD approach returns in any case a lower value of shear based force $F_b$. Regardless of the dowel diameter, this difference appears to be quite uniform, the DBD base shear being approximately 50% lower than that estimated using FBD; and again the only significant exception is case C/II.

Apparently, DBD results in less demanding design strength requirements. To evaluate this outcome critically, we must keep in mind that the base shear estimated by DBD is sensitive to the damping ratio, while FBD simply does not account for this parameter, roughly condensing into the q-factor all the information related to ductile and dissipative

**TABLE 3** Base-shear forces calculated according to Eurocode 8 [CEN, 2004]

| | CASE A | | CASE B | | CASE C | |
|---|---|---|---|---|---|---|
| | *Design I* | *Design II* | *Design I* | *Design II* | *Design I* | *Design II* |
| Seismic mass – $W$ [Kg] | 13600 | 13600 | 19800 | 19800 | 35500 | 35500 |
| Fundamental Period – $T$ [s] | 0.43 | 0.45 | 0.45 | 0.46 | 0.74 | 0.75 |
| Behavior factor – $q$ | 4 | 1.5 | 4 | 1.5 | 4 | 1.5 |
| Spectral acceleration – $S_a$[m s$^{-2}$] | 2.57 | 6.87 | 2.57 | 6.87 | 1.72 | 4.56 |
| **Design base shear – $F_b$ [KN]** | **35.1** | **93.6** | **50.9** | **135.8** | **61.2** | **161.8** |

capacity. For the specific technology, we have observed in Sec. 3.3 that the equivalent damping ratio is relatively high respect to other types of timber structures, due to the high energy dissipated by the joint during ductile deformation. DBD simply allows the designer to take proper account of this feature, while FBD summarizes into the q-factor all this information. The sharpest difference between the two design methods is observed for case C/II: in this case the size of the portal, which is very large with respect to the other cases, allows a relatively large displacement, equal to 188 mm using the conservative Eq. (11), for equal drift. This feature is properly taken into account by DBD, which results in a lower design base shear, but again is not considered in the classic FBD.

## 5. Conclusion

An application of Priestley's DBD method to a two-hinged glulam timber frame structure has been presented. A necessary condition for applying this method is that it be possible to estimate a priori (i) the target displacement $\Delta_d$ of the portal and (ii) the equivalent damping ratio $\xi_{eq}$ of the structure at the ultimate capacity. Both of these parameters can be derived from the geometrical dimensions of members and connections. We proposed a practical expression that allows us to calculate the ultimate target displacement and the equivalent viscous damping, simply and reliably. The expressions are very easy to use, and can be extended to a broader range of structural schemes. Using pushover nonlinear analyses, we demonstrated that the expression provides prior values of target displacement that are quite close to those obtained a posteriori using a much more refined model that takes account of the exact geometry of members and connections, as well as of the effect of the gravitational load. To estimate the equivalent damping ratio, we acknowledged the same formal approach proposed by Priestley, whereby the total energy dissipation is seen as the combination of a nominal viscous damping and a hysteretic damping function of the ductility demand. We calibrated the parameters involved in this formulation using the outcomes of an experimental campaign.

The comparison with the results of Eurocode 8 shows that the DBD method allows in the present case base shear forces significantly lower than FBD, despite the two methods being applied with consistent initial design assumptions. Although this outcome might give the impression that DBD is always less demanding than FBD, we must be very careful before generalizing this result. Once again we must remark that this specific result is due to the high dissipation capacity inherent to dowel connection technology, which apparently is conservatively valued in the q-factor based method of Eurocode 8. The examples reported show that the design base shear is very sensitive to the effective damping: this variability can be more easily controlled using a displacement-based procedure rather than a force-based one. We must also remark that for the specific type of connection investigated in this article we were able to take advantage of existing results, while the technical literature lacks experimental data that allow definition of general dissipation models to apply to other types of timber connections. Indeed, we must recognize that the real advantage of DBD over FBD is to allow the designer to treat correctly all the parameters involved in seismic design, which are elsewhere conservatively included in the force-reduction factor.



## Acknowledgments

This work was carried out with the financial contribution of the Italian Earthquake Engineering Laboratory Network (RELUIS), Project Reluis-DPC 2005-2008, Line IV, "Development of a Model Code for Direct Displacement-Based Seismic Design." The

authors wish to thank all the researchers who contributed to development of the formulation reported in this article, and specifically Gianni Giuliani, Tiziano Sartori, Andrea Polastri, and Timothy Sullivan.

## References

Anderson, G. T. [2001] "Experimental investigation of group action factor for bolted wood connections," Masters' Thesis, Virginia Polytechnic Institute and State University, Blacksburg, Virginia.

Blandon, C. A. and Priestley, M. J. N. [2005] "Equivalent viscous damping equations for direct displacement based design," *Journal of Earthquake Engineering* **9**, 257–278.

CEN [2000] "EN 14080: Timber structures. Glued laminated timber. Requirements," European Committee for Standardisation, Bruxelles, Belgium.

CEN [2001] "EN 12512: Timber structures – Test methods – Cyclic testing of joints made with mechanical fasteners," European Committee for Standardization, Bruxelles, Belgium.

CEN [2004a] "Eurocode 8: Design of structures for earthquake resistance. Part 1-1: General rules, seismic actions and rules for buildings," European Committee for Standardization, Bruxelles, Belgium.

CEN [2004b] "Eurocode 5: Design of timber structures. Part 1-1: General-Common rules and rules for buildings," European Committee for Standardization, Bruxelles, Belgium.

Chui, Y. H. and Smith, I. [1989] "Quantifying damping in structural timber components," *Proc. of the 2nd Pacific Timber Engineering Conference*, Auckland, New Zealand.

Chui, Y. H. and Yantao, L. [2005] "Modeling timber moment connection under reversed cyclic loading," *Journal of Earthquake Engineering* **13**(11), 1757–1763.

Chui, Y. H., Ni, C., and Jiang, L. [1998] "Finite-element model for nailed wood joints under reversed cyclic load," *Journal of Structural Engineering* **124**(1), 96–103.

Daneff, G., Smith, I., and Chui, Y. H. [1996] "Test protocol for evaluating seismic behavior of connections, *Proc. of International Wood Engineering Conference*, New Orleans, Louisiana.

Dolan, J. D., Blass, H. J., Ceccotti, A., Dyrbye, C., Gnuschke, M., Hansen, K. F., Nielsen, J., Ohlsson, S., Parche, M., Reyer, E., Stieda, C. K. A., Vergne, A., Vignole, A., and Yasumura, M. [1994] "Timber structures in seismic regions RILEM State-of-the-art Report," *Materials and Structures* **27**, 157–184.

Dolan, J. D. and Gutshall, S. T. [1997] *Cyclic Lateral Dowel Connection Tests for Seismic Evaluation. Earthquake Performance and Safety of Timber Structures*, Forest Products Society, Madison, Wisconsin.

Dowell R. K., Seible F., and Wilson E. [1998] "Pivot hysteresis model for reinforced concrete members," *Aci Structural Journal* **95**(5), 607–617.

Filiatrault, A. and Folz, B. [2002] "Performance-based seismic design of wood framed buildings," *Journal of Structural Engineering* **128**(1), 39–47.

Filiatrault, A., Isoda, H., and Folz, B. [2003] "Hysteretic damping of wood framed buildings," *Engineering Structures* **25**, 461–471.

Foliente, G. C. [1995] "Hysteresis modeling of wood joints and structural systems," *Journal of Structural Engineering* **121**, 1013–1022.

Foschi, R. O. and Bonac, T. [1974] "Load-slip characteristic for connections with common nails," *Wood Science* **9**(3), 118–123.

Gulkan, P. and Sozen, M. A. [1974] "Inelastic response of reinforced concrete structures to earthquake motions," *ACI Structural Journal* **71**, 604–610.

Heine, C. P. [2001] "Simulated response of degrading hysteretic joints with slack behavior," Ph.D. thesis, Wood Science and Forest Products, Virginia Polytechnic Institute and State University, Blacksburg, Virginia.

Heine, C. P. and Dolan, J. D. [2001] "A new model to predict the load-slip relationship of bolted connections in timber," *Wood and Fiber Science* **33**, 534–549.

Johansen K. W. [1949] "Theory of timber connections," *International Association of Bridge and Structural Engineering* **9**, Bern, Switzerland.

Loss, C. [2007] "Il direct displacement based design applicato a strutture di legno intelaiate: analisi numerico-probabilistica per la calibrazione di una metodologia di calcolo," Master's Thesis, University of Trento, Italy.

Pampanin, S., Palermo, A., Buchanan, A., Fragiacomo, M., and Deam, B. [2006] "Code provisions for seismic design of multi-storey post-tensioned timber buildings," *Proc. of International Council for Research and Innovation in Building and Construction*, Florence, Italy.

Patton-Mallory, M., Smith, F., Pellicane, P. J. [1998] "Modeling bolted connections in wood: a three-dimensional finite-element approach," *Journal of Testing and Evaluation* **26**(2), 115–124.

Piazza, M., Tomasi, R., and Modena, R. [2005] *Strutture in Legno. Materiale, Calcolo e Progetto Secondo le Nuove Normative Europee*, Hoepli, Milan, Italy.

Polastri, A., Tomasi, R., Piazza, M., and Smith, I. [2008] "Ductility of moment resisting dowelled connections in heavy timber structures," *Proc. of International Council for Research and Innovation in Building and Construction CIB-W18*, St. Andrews, Canada.

Polensek, A. and Bastendorff, K. M. [1987] "Damping in nailed joints of light-frame wood buildings," *Wood and Timber Science* **19**(2), 110–125.

Priestley, M. J. N. [1998] "Displacement-based approaches to rational limit states design of new structures," *Proc. of the 11th European Conference on Earthquake Engineering*, Paris, France.

Priestley, M. J. N. [2003] *Myths and Fallacies in Earthquake Engineering Revisited*, The Mallet Milne Lecture, IUSS Press, Pavia, Italy.

Sartori, T. [2008] "Comportamento dissipativo di giunti a completo ripristino nelle strutture di legno, Analisi numerico-sperimentale per l'applicazione alla progettazione sismica DDBD," Master's Thesis, University of Trento, Italy.

Smith, I., Daneff, G., Ni, C., and Chui, Y. H. [1998] *Performance of Bolted and Nailed Timber Connections Subjected to Seismic Loading*, Forest Products Society, Madison, Wisconsin.

Smith, I., Foliente, G., Nguyen, M., and Syme, M. [2005] "Capacities of dowel-type fastener joints in Australian pine," *Journal of Materials in Civil Engineering* **17**, 664–675.

Vanmarcke, E. H., Fenton, G. A., and Heredia-Zavoni, E. [1997] *SIMQKE-II, Conditioned Earthquake Ground Motion Simulator: Uuser's Manual, Version 2*, Princeton University, Princeton, New Jersey.

Yasamura, M. [1996] "Evaluation of seismic performance of timber structures," *Proc. of International Wood Engineering Conference*, New Orleans, Louisiana.

Yeh, C. T., Hartz, B. J., and Brown, B. [1971] "Damping sources in wood structures," *Journal of Sound and Vibration* **19**(4), 411–419.